2019

Predictive Peridynamic 3D Models of Pitting Corrosion in Stainless Steel with Formation of Lacy Covers

Siavash Jafarzadeh
University of Nebraska-Lincoln, sjafarzadeh@huskers.unl.edu

Florin Bobaru
University of Nebraska-Lincoln, fbobaru2@unl.edu

Ziguang Chen
Huazhong University of Science and Technology, Wuhan, China

Paper No.
13374

NACE INTERNATIONAL
CORROSION Conference & Expo 2019

Predictive Peridynamic 3D Models of Pitting Corrosion in Stainless Steel with Formation of Lacy Covers

Siavash Jafarzadeh, Florin Bobaru
University of Nebraska-Lincoln, Lincoln, NE, 68588-0526, USA

Ziguang Chen
Huazhong University of Science and Technology, Wuhan 430074, China

ABSTRACT

In this work, the peridynamic corrosion model is used for 3D simulation of pitting corrosion in stainless steel. Models for passivation and salt layer formation are employed to predict detailed characteristics of pit growth kinetic in stainless steels, such as lacy cover formation on top of the pit, and the diffusion-controlled regime at the pit bottom. The model is validated against an experimentally grown pit on 316L stainless steel in NaCl solution. Lacy covers in this model are formed autonomously during the simulation process. They are remarkably similar to the covers observed on top of the real pits.

Key words: peridynamics, pitting corrosion, stainless steel, lacy cover, passivation, salt layer

INTRODUCTION

Corrosion in stainless steel (SS) is of significant interest due to the wide application of this alloy, with high mechanical strength and good corrosion resistance, in various industries. Pitting corrosion in SS takes the form of localized pits growing under perforated (lacy) covers.[1-6] Covered pits are difficult to spot, and they can maintain stable growth.[6] Since stable pits are potential sites for crack initiation, and can lead to catastrophic failure due to stress-corrosion cracking,[7] predictive models for pitting corrosion in stainless steel are of great importance. Such models could also be used to reveal the mechanisms of localized corrosion, and can help engineers and material scientists with finding new methods to stop or slow down damage progression under mechanical loading and environmental conditions.

While many models exist for pitting corrosion, there exist a few that take into account the lacy cover on top of the pits in stainless steels. Most of these models include the lacy cover as a given, known boundary condition, and study pit growth under such covers,[8-11]. However, lacy covers influence pit growth and also are influenced by it, meaning that they should be obtained as part of the solving procedures, not enforced as pre-determined boundary conditions. There are only a couple of studies that model the actual formation of perforated pit covers.[12-14] Simulations in these studies are either in 2D, or axisymmetric, which are different from the general 3D conditions.

In this study, a passivation criterion[14] is used within the 3D peridynamic corrosion-damage model[12, 15], to predict the autonomous formation of lacy covers during the pitting process in stainless steel.

MODEL DESCRIPTION

In this section, the peridynamic theory for corrosion damage is briefly reviewed and the model is presented. Then, the passivation and salt-layer models with application to modeling pitting corrosion in stainless steel are discussed.

Peridynamic Theory

The theory of peridynamics (PD) is a nonlocal formulation of continuum mechanics which is especially useful for modeling of static and dynamic fracture and damage problems.[16-18] Governing equations in this non-local framework are in the form of integro-differential equations. Contrary to partial differential equations used to describe classical local models, integro-differential equations do not require the smoothness nor the continuity of the unknown fields. This a significant advantage in modeling problems with evolving discontinuities such as crack propagation,[19-23] and corrosion progression.[8, 12, 15, 24, 25] Note that a crack is a discontinuity in displacement field, and a corrosion front is a discontinuity between the metal and electrolyte phases.

In the PD theory, each material point $\boldsymbol{x}$, interacts with other material points $\hat{\boldsymbol{x}}$ in its neighborhood. The neighborhood is usually a sphere in 3D, centered at $\boldsymbol{x}$ called the *Horizon of* $\boldsymbol{x}$ ($H_{\boldsymbol{x}}$). The radius of this sphere is called *horizon-size* and is denoted by δ.

In classical local models, materials behavior is modeled via using relationships between various quantities and derivatives of those quantities, at each point. In PD, models are developed by describing the characteristics of pair-wise interactions of each point $\boldsymbol{x}$ with its neighbor points $\hat{\boldsymbol{x}}$. In this nonlocal framework, the objects that carry each of these pairwise-interactions are called *bonds*. For example, in PD diffusion equation for heat/mass-transfer, the transfer from $\hat{\boldsymbol{x}}$ to $\boldsymbol{x}$ occurs via the $(\boldsymbol{x}, \hat{\boldsymbol{x}})$ "bond" (see Figure 1).

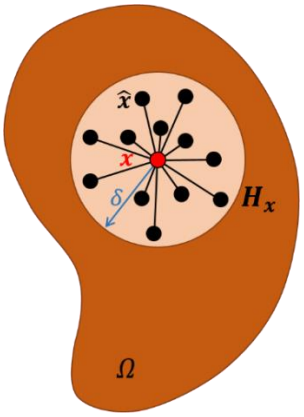

Figure 1. Schematic of a peridynamic body, and the nonlocal interactions of a generic point x within its neighborhood H_x.

Peridynamic Model for Corrosion Damage

Although PD was originally introduced for fracture problems,[18] it can also be used to model heat and mass transfer in bodies with evolving discontinuities.[26-28] The nonlocal diffusion for mass transfer, coupled with damage and phase-change models, is then employed to simulate the evolution of corrosion damage in solids.[15]

The coupled set of equations 1 to 4, is the PD model for corrosion-damage:

$$\frac{\partial C(\boldsymbol{x},t)}{\partial t} = \int_{H_x} k(\boldsymbol{x},\hat{\boldsymbol{x}},t)\frac{C(\hat{\boldsymbol{x}},t)-C(\boldsymbol{x},t)}{\|\hat{\boldsymbol{x}}-\boldsymbol{x}\|^2}\,dV_{\hat{x}} \tag{1}$$

$$k(\boldsymbol{x},\hat{\boldsymbol{x}},t) = \begin{cases} k_{\mathrm{L}} = \dfrac{9K_{\mathrm{L}}}{2\pi\delta^3} & ,d(\boldsymbol{x},t)=1 \;\&\; d(\hat{\boldsymbol{x}},t)=1 \\ 0 & ,d(\boldsymbol{x},t)<1 \;\&\; d(\hat{\boldsymbol{x}},t)<1 \\ k_{\mathrm{diss}} & ,[d(\boldsymbol{x},t)\ or\ d(\hat{\boldsymbol{x}},t)]<1 \;\&\; [d(\boldsymbol{x},t)\ or\ d(\hat{\boldsymbol{x}},t)]=1 \end{cases} \tag{2}$$

$$d(\boldsymbol{x},t) = \begin{cases} 1 & ,C(\boldsymbol{x},t) \le C_{\mathrm{sat}} \\ \dfrac{C_{\mathrm{solid}}-C(\boldsymbol{x},t)}{C_{\mathrm{solid}}-C_{\mathrm{sat}}} & ,C_{\mathrm{sat}} < C(\boldsymbol{x},t) < C_{\mathrm{solid}} \\ 0 & ,C(\boldsymbol{x},t)=C_{\mathrm{solid}} \end{cases} \tag{3}$$

$$d(\boldsymbol{x},t) = \frac{\int_{H_x}[1-\mu(\boldsymbol{x},\hat{\boldsymbol{x}},t)]\,dV_{\hat{x}}}{\int_{H_x} dV_{\hat{x}}} \tag{4}$$

Equation 1 is the PD diffusion equation, $C(\boldsymbol{x},t)$ is the concentration of metal atoms at point $\boldsymbol{x}$ and time t, $dV_{\hat{x}}$ is the differential volume at $\hat{\boldsymbol{x}}$, and $k(\boldsymbol{x},\hat{\boldsymbol{x}},t)$ is the micro-diffusivity of $(\boldsymbol{x},\hat{\boldsymbol{x}})$ bond at time t. In the PD corrosion damage model, k is a damage-dependent scalar, and is calculated from Equation 2. In this model, $d(\boldsymbol{x},t)$ is the *damage* caused by the corrosion/dissolution process, and is a real-valued scalar varying between 0 and 1. When $d=1$, that denotes the liquid phase, and if $d<1$, that denotes the solid phase. Equation 2 states that for bonds with both ends in the solid phase, k is zero; for bonds with both ends in the liquid electrolyte, k is k_{L} and is calculated from the classical diffusivity of the electrolyte (K_{L}). For interfacial bonds with one end in the liquid and one end in the solid, k is equal to k_{diss}, which is the quantity that controls the interfacial solid-to-liquid mass flux. Since k_{diss} drives the dissolution and determines the corrosion kinetics, it is called the *dissolution parameter*. k_{diss} can be easily calibrated to the current density measured from the activation-controlled anodic reaction in the corrosion process.[12] Progression of corrosion is modeled via a concentration-dependent definition of damage in Equation 3. In this equation, C_{solid} is the concentration of metal atoms in the intact solid phase, and C_{sat}, is the saturation concentration of oxidized metal atoms in the electrolyte. The function $\mu(\boldsymbol{x},\hat{\boldsymbol{x}},t)$ in Equation 4, is defined as a history-dependent binary scalar-field (equal to either 0 or 1). Damage in PD fracture models is a function of μ, which determines whether a bond is intact and is able to carry mechanical force ($\mu=1$), or that the bond is broken and is unable to carry force ($\mu=0$). In the PD coupled corrosion-damage model, the set of equations 1 to 4 need to be solved for $C(\boldsymbol{x},t)$ and $\mu(\boldsymbol{x},\hat{\boldsymbol{x}},t)$. Details of the model derivation are available in the literature.[15, 24]

Note that the described set of equations is the general PD corrosion model. For different types of corrosion, like pitting, intergranular, etc., the appropriate function $k(\boldsymbol{x},\hat{\boldsymbol{x}},t)$ should be specified, as particular "constitutive models" for each of the corrosion types.[12, 24]

Peridynamic Model for Pitting Corrosion in Stainless Steel

In the case of pitting corrosion in stainless steel, three mechanisms exist that have major contributions to the overall evolution of corrosion damage in these materials. In particular, to the formation of localized pits, growing under lacy covers. These *mechanisms* are: 1) partial passivation of pit walls and active underneath corrosion; 2) undercutting the passive surface and pore formation; and 3) salt layer presence and diffusion-controlled corrosion at the pit bottom.[3-6, 29, 30]

Partial passivation of the pit walls are due to the local acidity drop close to the pit mouth, in response to the low concentration of oxidized metal atoms in that location.[31] Corrosion underneath the passive region continuous and once reached the surface, the thin (nano-meter thick) passive film breaks and the pores are created.[6, 30, 32]

Diffusion controlled regime at the pit bottom is the result of salt-layer formation when dissolution flux exceeds the diffusion flux in the pit, and saturates the electrolyte.[29] The salt-layer presence reduces the local corrosion rate and balances the dissolution flux with the diffusion flux.[29]

Three simple models have been proposed to implement these mechanisms within a PD corrosion damage model.[12] The models were used with a 2D formulation to simulate pitting corrosion on the edge of a 304 stainless steel foil.[12] Here, the brief descriptions of these models are given. The details are available in that study.[12]

Passivation Model

Using a concentration-based criterion for passivation,[14] when the concentration of oxidized atoms at a liquid point near the corrosion front drops below a critical value (C_{crit}), the solid region in the horizon of that liquid point (if any) is passivated. This is done by assigning a permanent zero value to k_{diss} for the interfacial bonds, connected to the passivated region. With this model, the passive region stops being corroded.

Passive-film Rupture Model

To model the passive film break down at pore locations, the passive region in the PD model is simply removed when it is fully surrounded by the electrolyte from both sides: outside and inside of the pit. Details are available in the reference.[12]

Salt-layer Model

To model the effect of salt-layer presence, when the concentration at a liquid node near the corrosion front exceeds C_{sat}, then corrosion of the solid region inside the horizon of that liquid node (if any) is stopped temporarily. Dissolution can resume when the concentration of that oversaturated liquid node drops back to a value below C_{sat} due to out-diffusion from the pit. Consecutive corrosion “stop-and-go” in interfacial bonds connected to oversaturated nodes, occurs within the small time steps (milliseconds), and makes the dissolution flux follow the diffusion in the electrolyte in the global corrosion time-scale, as one would expect from the diffusion-controlled regime. See the reference for details.[12, 33]

Discretization and Numerical Method

For 3D simulations, the spatial domain is discretized with a uniform grid. To solve corrosion progression in time, total time is also divided into equal time steps. At each time step, one-point Gaussian integration is used to perform the spatial quadrature in Equation 1. Then, the Forward Euler method is used to update the concentration values for the next time increment. Damage and micro-diffusivity values are then updated according to Equations 2 and 3. A special stochastic procedure is used to update μ values for each bond.[15] This novel stochastic procedure, introduces a randomness in shape of the computed corrosion pits similar to one observed experimentally in materials in which heterogeneity is relatively small. This micro-scale randomness represents some of the micro-structural heterogeneity of the material which is not explicitly included in the model.[12] Note that the overall characteristics of the corrosion, like the pit size and the rate of dissolution remains deterministic.[12] Specifics of the discretization schemes, the numerical procedures, and the stochastic scheme are found elsewhere.[15, 24]

RESULTS AND DISCUSSION

In this section, the 3D model is validated against a published experiment on pitting corrosion in 316L stainless steel.[34]

Experiment Description

This experimentally observed pit is grown at room temperature, in 0.1 M NaCl solution, under potentiostatic condition of applied 700 mV potential (vs SCE).[34] The activation-controlled current density is measured as 53 KA.m^{-2} at pit initiation.[34]

Computational Model Setup

In this part, the selection of the model parameters is discussed. Then, the discretized model with specific initial and boundary conditions is provided.

Model Parameter Selection

Given the composition of the 316L alloy,[34] and knowing the density and molar mass for each element, C_{solid} for the alloy is calculated to be 163,200 mol.m^{-3}. C_{sat} value for oxidized metal atoms in NaCl solution at room temperature is taken 4,600 mol.m^{-3} which is measured from dissolution of $FeCl_2$ salt in water.[35] Diffusivity in the liquid phase, K_{L}, is taken to be the diffusivity of Fe^{2+} ions in the electrolyte, which is calculated to be 8.6×10^{-10} m^2.s^{-1} for room temperature.[35] The critical value (C_{crit}) for the passivation criterion is reported to be about 2,500 mol.m^{-3}.[36]

The dissolution parameter for interfacial bonds needs to be calibrated for this metal-electrolyte system. According to the given activation-controlled current density 53 KA.m^{-2}, k_{diss} is calibrated to be 4.3×10^{4} m^{-1}.s^{-1}. The details of the calibration procedure are explained in literature.[12, 15]

Note that once, k_{diss} is calibrated for a specific potential and metal-electrolyte system, simulation of corrosion under other potential values are also possible, according to the Tafel equation.[12, 15]

Discretized 3D Model and Initial and Boundary Conditions

The domain of the computational model is a $120\times120\times100$ μm^3 cuboid. Similar to the 2D simulation case in another study,[12] the horizon size (δ) is selected to be 4 μm.

This domain is discretized using a uniform grid with 1 μm grid-spacing in each of the three dimensions. Inclusions and imperfections on the passive film are understood to be the reasons for pit initiation.[37, 38] To model the initiation, a spherical initial pit with radius 5 μm, filled with C_{sat} is placed at the center of the top surface of the domain. The metal concentration value in the rest of the domain is C_{solid}(representing the intact, bulk solid).

The boundary condition at the top surface is constant zero metal concentration. This condition mimics the presence of a dilute bulk electrolyte outside of the pit. No-flux boundary conditions are imposed on the sides and bottom of the corroding domain. Details of imposing boundary conditions in nonlocal models are found in literature.[27, 39, 40]

Time step in this simulation is selected as 0.001 s, in order to maintain the stability of the Forward Euler scheme for time integration.

Simulation Results

Using the model and the input parameters mentioned above, a 3D PD simulation is performed for 100 seconds (physical time) of pit growth in 316 stainless steel. Figure 2 shows the evolution of metal concentration through a median cross-section of the domain. The interplay between

passivation and perforation stages are observed during the pit growth. The noticed dish-shape geometry of the pit is due to the salt-layer model under diffusion-controlled regime.

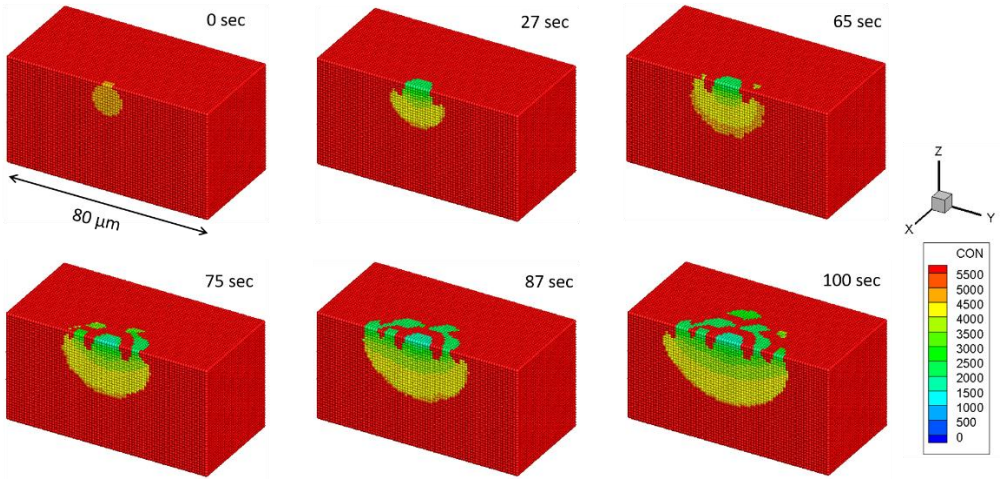

Figure 2. Snapshots for the time-evolution of metal concentration obtained by the 3D peridynamic simulation for pitting corrosion in 316L stainless steel in 0.1 M NaCl solution, under application of 700 mV(SCE) for 100 seconds. Autonomous formation of lacy cover on top of the pit is noticed due to repeated passivation and perforation events.

Note that the lacy cover is formed autonomously during the simulation process, due to the models for passivation and the passive-film rupture, incorporated into the general PD corrosion model.

Figures 3a and 3b, are respectively the lacy covers of the real and the simulated pits. Figure 3c shows the 3D visualization of the underneath pit morphology obtained by the peridynamic computational model. The pit shape and depth-to-width aspect ratio are in the range of the values reported in 3D experimental observations for covered pits in stainless steels.[1, 41, 42]

Similar patterns are noticed between the simulated and the experimental lacy cover, such as the narrow piecewise perforations along different segments. This type of predictions of the lacy cover formation are unique, to the best of the authors' knowledge. The reason for the asymmetric cover and random distribution of pores in it is the stochastic procedure used in solving equations 3 and 4.[15, 24] Note that the randomness acts at the bond-level and the main characteristics of the pit, like growth rate, depth-to-width aspect ratio, and porosity of the cover are deterministic.[12, 24]

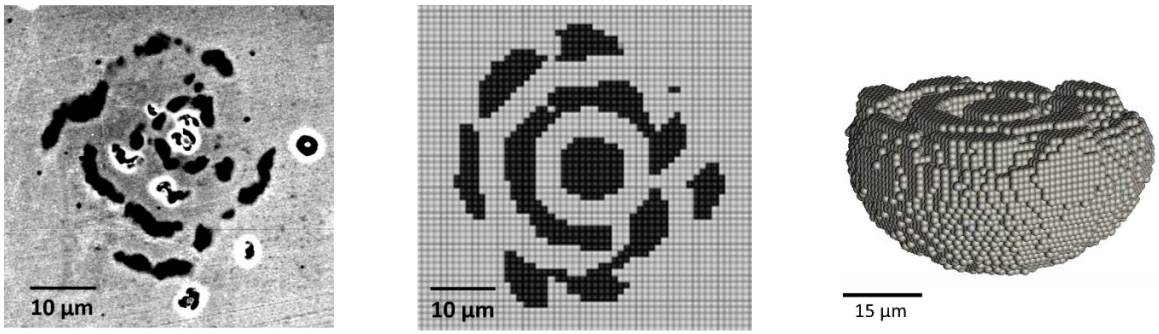

(a) (b) (c)

Figure 3. a) Lacy cover of the experimental corrosion pit grown on 316L stainless steel in 0.1 M NaCl at 700 mV (SCE); b) Lacy cover from the 3D peridynamic simulation of pitting corrosion for the same material and environment; c) the 3D under-cover pit from the peridynamic simulation.

CONCLUSIONS

In this study, the peridynamic coupled corrosion-damage model is used to perform a 3D simulation for pitting corrosion in stainless steel. Models for passivation, passive-film rupture, and salt-layer formation are incorporated into the general 3D PD corrosion-damage model to predict the details of the pitting corrosion process in stainless steel. The PD model is able to uniquely reproduce the lacy cover complex morphology on top of the pit observed experimentally. The model is validated against an experimental pit in 316L stainless steel in NaCl solution under potentiostatic condition. The pit shape is also found to be in agreement with experimental observations for other covered pits in stainless steel.[1, 33] The relatively complex phenomena of formation of lacy covers in pitting corrosion are well reproduced by the model described in this paper, a model that probably uses the smallest possible set of input data: activation-controlled current density, diffusivity of the electrolyte, and concentration-based criteria for saturation and passivation. The validated simulation results suggest that the PD corrosion-damage model is a promising tool for engineers and scientists concerned with the mechanisms and kinetics of localized corrosion in stainless steels.

ACKNOWLEDGEMENTS

This work has been supported by the ONR project “SCC: the Importance of Damage Evolution in the Layer Affected by Corrosion” (program manager William Nickerson), and by the AFOSR MURI Center for Materials Failure Prediction through Peridynamics (program managers David Stargel, Ali Sayir, Fariba Fahroo, and James Fillerup). This work was completed utilizing the Holland Computing Center of the University of Nebraska, which receives support from the Nebraska Research Initiative.

REFERENCES

1. F. Almuaili, "Characterisation of 3d Pitting Corrosion Kinetics of Stainless Steel in Chloride Containing Environments" University of Manchester,
2. M. Ghahari, D. Krouse, N. Laycock, T. Rayment, C. Padovani, M. Stampanoni, F. Marone, R. Mokso, A.J. Davenport, *Corrosion Science* 100, (2015): p. 23-35.
3. P. Ernst, R. Newman, *Corrosion Science* 44, 5 (2002): p. 927-941.
4. P. Ernst, R. Newman, *Corrosion science* 44, 5 (2002): p. 943-954.
5. P. Ernst, N. Laycock, M.H. Moayed, R. Newman, *Corrosion science* 39, 6 (1997): p. 1133-1136.
6. P. Pistorius, G. Burstein, *Philosophical Transactions of the Royal Society of London A: Mathematical, Physical and Engineering Sciences* 341, 1662 (1992): p. 531-559.
7. F. Delaunois, A. Tshimombo, V. Stanciu, V. Vitry, *Corrosion Science* 110, (2016): p. 273-283.
8. Z. Chen, G. Zhang, F. Bobaru, *Journal of The Electrochemical Society* 163, 2 (2016): p. C19-C24.
9. A. Vagbharathi, S. Gopalakrishnan, *Proc. R. Soc. A* 470, 2168 (2014): p. 20140001.
10. S. Scheiner, C. Hellmich, *Computer Methods in Applied Mechanics and Engineering* 198, 37-40 (2009): p. 2898-2910.
11. S. Scheiner, C. Hellmich, *Corrosion science* 49, 2 (2007): p. 319-346.
12. S. Jafarzadeh, Z. Chen, F. Bobaru, *Corrosion* 44, 4 (2018): p. 393-414.

13. N. Laycock, S. White, *Journal of the Electrochemical Society* 148, 7 (2001): p. B264-B275.
14. N. Laycock, S. White, J. Noh, P. Wilson, R. Newman, *Journal of the electrochemical society* 145, 4 (1998): p. 1101-1108.
15. Z. Chen, F. Bobaru, *Journal of the Mechanics and Physics of Solids* 78, (2015): p. 352-381.
16. F. Bobaru, J.T. Foster, P.H. Geubelle, S.A. Silling, *Handbook of Peridynamic Modeling*, CRC press, 2016).
17. S.A. Silling, R. Lehoucq, in *Peridynamic Theory of Solid Mechanics*, ed., vol. 44 Elsevier, 2010), p. 73-168.
18. S.A. Silling, *Journal of the Mechanics and Physics of Solids* 48, 1 (2000): p. 175-209.
19. G. Zhang, G.A. Gazonas, F. Bobaru, *International Journal of Impact Engineering* 113, (2018): p. 73-87.
20. Z. Xu, G. Zhang, Z. Chen, F. Bobaru, *International Journal of Fracture* 209, 1-2 (2018): p. 203-222.
21. J. Mehrmashhadi, Y. Tang, X. Zhao, Z. Xu, J. Pan, Q. Van Le, F. Bobaru, *IEEE Transactions on Components, Packaging and Manufacturing Technology*, (2018):
22. Z. Chen, S. Niazi, G. Zhang, F. Bobaru, in *Peridynamic Functionally Graded and Porous Materials: Modeling Fracture and Damage*, ed.Springer, 2018), p. 1-35.
23. W. Hu, Y.D. Ha, F. Bobaru, *International Journal for Multiscale Computational Engineering* 9, 6 (2011):
24. S. Jafarzadeh, Z. Chen, F. Bobaru, *Journal of The Electrochemical Society* 165, 7 (2018): p. C362-C374.
25. D. De Meo, E. Oterkus, *Ocean Engineering* 135, (2017): p. 76-83.
26. J. Zhao, Z. Chen, J. Mehrmashhadi, F. Bobaru, *International Journal of Heat and Mass Transfer* 126, (2018): p. 1253-1266.
27. S. Oterkus, E. Madenci, A. Agwai, *Journal of Computational Physics* 265, (2014): p. 71-96.
28. F. Bobaru, M. Duangpanya, *Journal of Computational Physics* 231, 7 (2012): p. 2764-2785.
29. H. Isaacs, J.H. Cho, M. Rivers, S. Sutton, *Journal of The Electrochemical Society* 142, 4 (1995): p. 1111-1118.
30. G. Frankel, L. Stockert, F. Hunkeler, H. Boehni, *Corrosion* 43, 7 (1987): p. 429-436.
31. G. Gaudet, W. Mo, T. Hatton, J. Tester, J. Tilly, H.S. Isaacs, R. Newman, *AIChE journal* 32, 6 (1986): p. 949-958.
32. W. Tian, N. Du, S. Li, S. Chen, Q. Wu, *Corrosion Science* 85, (2014): p. 372-379.
33. S. Jafarzadeh, Z. Chen, J. Zhao, F. Bobaru, *Pitting, lacy covers, and pit merger in stainless steel: 3D peridynamic models (in review)*.
34. M. Zakeri, D. Nakhaie, M. Naghizadeh, M.H. Moayed, *Corrosion Science* 93, (2015): p. 234-241.
35. N. Laycock, R. Newman, *Corrosion Science* 40, 6 (1998): p. 887-902.
36. S. Ghahari, D. Krouse, N. Laycock, T. Rayment, C. Padovani, T. Suter, R. Mokso, F. Marone, M. Stampanoni, M. Monir, *Corrosion Engineering, Science and Technology* 46, 2 (2011): p. 205-211.
37. S. Zheng, Y. Wang, B. Zhang, Y. Zhu, C. Liu, P. Hu, X. Ma, *Acta Materialia* 58, 15 (2010): p. 5070-5085.
38. T.S.L. Wijesinghe, D.J. Blackwood, *Corrosion Science* 49, 4 (2007): p. 1755-1764.
39. B. Aksoylu, F. Celiker, O. Kilicer, *Advances in Computational Mathematics*, (2018): p. 1-40.
40. Q. Le, F. Bobaru, *Computational Mechanics*, (2017): p. 1-20.

41. F. Almuaili, S. McDonald, P. Withers, A. Cook, D. Engelberg, *Corrosion Science* 125, (2017): p. 12-19.
42. S.M. Ghahari, A.J. Davenport, T. Rayment, T. Suter, J.-P. Tinnes, C. Padovani, J.A. Hammons, M. Stampanoni, F. Marone, R. Mokso, *Corrosion Science* 53, 9 (2011): p. 2684-2687.